5376 *Inorg. Chem.* **2009**, *48*, 5376–5381
DOI: 10.1021/ic900369b

Inorganic Chemistry
Article

Experimental Insight into the Radiation Resistance of Zirconia-Based Americium Ceramics

Renaud C. Belin,*,† Philippe M. Martin,† Philippe J. Valenza,† and Andreas C. Scheinost‡

†*CEA, DEN, DEC, CEN Cadarache F-13108 Saint-Paul-Lez-Durance, France, and* ‡*Forschungszentrum Dresden-Rossendorf (FZD), Institute of Radiochemistry, P.O. Box 510119, 01314 Dresden, Germany*

Received February 23, 2009

Our works shows that the americium pyrochlore $^{241}Am_2Zr_2O_7$ undergoes a phase transition to a defect-fluorite structure along with an unusual volume contraction when subjected to internal radiation from α-emitting actinides. Disorder relaxation proceeds through the simultaneous formation of cation antisites and oxygen Frenkel pairs. X-ray absorption spectroscopy at the Am−L_{II} and the Zr−K edges reveals that Am−O polyhedra show an increasing disorder with increasing exposure. In contrast, the Zr−O polyhedral units remain highly ordered, while rotating along edges and corners, thereby reducing the structural strain imposed by the growing disorder around americium. We believe it is this particular property of the compound that provides the remarkable resistance to radiation (>9.4×10^{18} α-decay events g^{-1} or 0.80 dpa).

Introduction

Ceramics intended for use as nuclear fuels, transmutation targets, or actinide immobilization matrices have to withstand severe conditions including internal radiation. Resistance to amorphization and limited swelling are therefore key requirements. Oxygen-deficient compounds with structures related to fluorite often meet these criteria. Pyrochlore oxides with the formula $A_2B_2O_7$ (A and B are metallic cations) are especially appealing because they are able to host high amounts of actinides. The ratio of the two cation radii, r_A/r_B, may vary between 1.46 and 1.78, thereby defining the stability field for pyrochlore. At the lower limit, cation disorder increases and the tendency of pyrochlore to transform into a defect-fluorite structure is higher.[1] Experiments have shown that this transition can be induced by irradiating selected $A_2^{3+}Zr_2^{4+}O_7$ pyrochlores, the resulting phase being highly radiation-resistant.[2] Up to now, most studies have been performed on surrogate rare-earth compounds using ion-beam irradiation in order to simulate α self-irradiation. This external irradiation induces only localized disturbed regions, whereas α-emitting actinides within the structure irradiate the compound homogeneously. However, due to the radiotoxicity of α-emitting actinides and the associated handling problems, such studies, which would represent realistic conditions much better, are rare.[3−6]

The order−disorder phase transition of pyrochlore to defect-fluorite was investigated by closely following structural changes of $^{241}Am_2Zr_2O_7$ under α self-irradiation. The presence of 62 wt % of ^{241}Am ($t_{1/2}$ = 432 y) in the structure provided a high dose rate which enabled us to follow within only four years an α self-irradiation-induced aging process corresponding to much longer time periods in the case of immobilization ceramics.[7] X-ray diffraction (XRD) and X-ray absorption spectroscopy (XAS) analyses were combined to selectively probe the long-range and the short-range order and the local environment of both cations.[8,9]

Materials and Methods

The displacements per atom (dpa) were calculated using SRIM (The Stopping and Range of Ions in Matter),[10] with the commonly accepted energy of 50 eV for the displacement of atoms in the pyrochlore structure.[1]

A few milligrams of $^{241}AmO_2$ and ZrO_2 powders were ground and mixed in the appropriate ratios and calcined in a molybdenum crucible under a reducing atmosphere (i.e., Ar/H_2) at 1673 K for 55 h. The entire process was repeated

*To whom correspondence should be addressed. Phone: +33 4 4225 4954. Fax: +33 4 4225 4717. E-mail: renaud.belin@cea.fr.

(1) Ewing, R.; Weber, W.; Lian, J. *J. Appl. Phys.* **2004**, *95*, 5949–5971.
(2) Wang, S.; Begg, B.; Wang, L.; Ewing, R.; Weber, W.; Kutty, K. *J. Mater. Res.* **1999**, *14*, 4470–4473.
(3) Lumpkin, G.; Ewing, R. *Phys. Chem. Miner.* **1988**, *16*, 2–20.
(4) Weber, W.; Wald, J.; Matzke, H. *J. Nucl. Mater.* **1986**, *138*, 196–209.
(5) Farnan, I.; Cho, H.; Weber, W. J. *Nature* **2007**, *445*, 190–193.
(6) Sykora, R.; Raison, P.; Haire, R. *J. Solid State Chem.* **2005**, *178*, 578–583.
(7) Weber, W.; Ewing, R.; Catlow, C.; de la Rubia, T.; Hobbs, L.; Kinoshita, C.; Matzke, H.; Motta, A.; Nastasi, M.; Salje, E.; Vance, E.; Zinkle, S. *J. Mater. Res.* **1998**, *13*, 1434–1484.
(8) Conradson, S.; Manara, D.; Wastin, F.; Clark, D.; Lander, G.; Morales, L.; Rebizant, J.; Rondinella, V. *Inorg. Chem.* **2004**, *43*, 6922–6935.
(9) Martin, P.; Grandjean, S.; Valot, C.; Carlot, G.; Ripert, M.; Blanc, P.; Hennig, C. *J. Alloys Compd.* **2007**, *444*−*445*, 410–414.
(10) Ziegler, J.; Biersack, J.; Littmark, U. *The Stopping and Range of Ions in Solids*; Pergamon Press: New York, 1985.

Published on Web 04/30/2009

twice. During the aging process, the $Am_2Zr_2O_7$ powder was stored in a hermetic container under an inert atmosphere (pure N_2) to prevent oxidation.

XRD measurements were performed at room temperature with a Bragg−Brentano Siemens D5000 X-ray diffractometer using a curved quartz monochromator and copper radiation from a conventional tube source (Kα1 radiation, λ = 1.5406 Å). Powder diffraction patterns were obtained by scanning from 25−148° 2Θ using 0.02° step intervals.

A preliminary Le Bail refinement was carried out. The scale factor and background parameters only were first refined, and then the cell parameter and fwhm parameters were varied. A pseudo-Voigt peak shape function was employed, and an asymmetry correction was applied in the form of a sum of five pseudo-Voigt peaks. The background was approximated by a Chebyshev polynomial function with 12 terms. The second step involved performing a Rietveld refinement[11] using JANA 2000[12] with a Newton−Raphson algorithm. The lattice parameter obtained from the Le Bail method was taken as the initial value and then concurrently refined as profile parameters and atomic coordinates. The R_p profile, R_{wp} weighted profile, and Bragg factors were calculated.

EXAFS measurements were performed at the Rossendorf Beamline (BM20) located at the European Synchrotron Radiation Facility (ESRF, Grenoble, France). EXAFS samples were prepared by mixing about 1 mg of material with 80 mg of boron nitride. Samples were then pressed into a thin bar so that the sample repartition could be optimized regarding the beam dimension. The pellet was then inserted into a hermetic Teflon container and, in addition, into a sealed polyethylene sample holder to provide a double confinement for safety reasons. Due to the maximum level of radioactivity authorized at the beamline (185 MBq), only one sample was kept at a time at the ESRF. Sample holders were mounted in a closed-cycle He cryostat running at 15 K.

Americium L_{II} (22952 eV) and zirconium K (17998 eV) edge spectra were collected for each sample in fluorescence mode using a 13-element Ge detector. The spectra were corrected for dead time using a measured relationship between the incoming count rate and selected channel analyzer readings for each channel using the SixPack software package. Energy calibrations were performed using a Zr foil or a Mo foil (20000 eV) positioned after the second ionization chamber. The ATHENA software[13] was used for extracting EXAFS oscillations from the raw absorption spectra. Experimental EXAFS spectra were Fourier-transformed using a Hanning window over the full k space range available for each edge: 2.1−13.3 $Å^{-1}$ for americium and 2.5−10.3 $Å^{-1}$ for zirconium. Curve fitting was performed in k^3 for R values in the range 1.3−4.1 Å for both edges. Phases and amplitudes for the interatomic scattering paths were calculated with the ab initio code FEFF8.20.[14] At the Zr edge, a multiscattering path corresponding to the doubling of the Zr−O single-scattering path (Zr−O−Zr−O) was fitted, correlating R and σ^2 to double the values used for the Zr−O single-scattering shell.

Both edges were simultaneously refined, with Am−Zr and Zr−Am distances initially constrained to the same values. In addition, coordination numbers for cation−cation shells were fixed at a value of 6.0. Once satisfactory results were obtained, the constraints were removed with no significant variation. Moreover, we attempted to introduce anharmonicity in the static disorder by adding skewness to the Am−O_{48f} and cation−cation paths with a third cumulant.[15] As this procedure did not improve the quality of the fit nor change the parameters obtained without a third cumulant, anharmonicity was disregarded.

Results and Discussion

As expected from the ionic radius ratio criterion (r_{Am}/r_{Zr} = 1.51), the compound gradually transformed to the defect-fluorite structure in about 370 days corresponding to 0.21 dpa (Figure 1). In contrast to the commonly observed increase in volume under α self-irradiation, for example, for $^{241}AmO_2$,[16] we found a decrease in the cell parameter by 0.02 Å, corresponding to a volume contraction of 0.6% (Figure 2). To our knowledge, such a volume reduction has never been observed before in irradiated pyrochlore. After the phase transition was completed, the volume remained constant. Within the whole experimental period of 1360 days, no amorphization was observed. The cumulated dose during this period was 9.4×10^{18} α-decay events g^{-1}, corresponding to 0.80 dpa. This is equivalent to the dose accumulated by multiphase ceramics with 20 wt % ^{239}Pu during 1000 years of storage.[7] The defect-fluorite structure is therefore remarkably resistant to such radiation doses.

What drives the resistance to radiation and the unusual negative lattice expansion observed in $Am_2Zr_2O_7$? We believe that the answer lies in a thorough understanding of how lattice point defects are formed and recombined during the order−disorder transition.

Atomistic simulations based on energy minimization techniques best describe the disorder transition by the formation of cation antisites and oxygen Frenkel pairs.[17,18] The $Am_2Zr_2O_7$ $Fd\bar{3}m$ cubic structure is a fluorite-type superstructure with doubled cell parameters, which can be regarded as two distinct cationic and anionic sublattices: Am occupies the 16*d* (1/2, 1/2, 1/2) site, Zr the 16*c* (0, 0, 0) site, and O the 8*b* (3/8, 3/8, 3/8) and 48*f* (*x*, 1/8, 1/8) sites. Only the "*x*" value of the O(48*f*) is unconstrained. The O site 8*a* (1/8, 1/8, 1/8) is vacant. In the defect-fluorite $Fd\bar{3}m$ structure, both Am and Zr occupy the 4a (0,0,0) site, while O is in 8*c* (1/4, 1/4, 1/4). Figure 3 shows coordination shells of Am and Zr cations in both structures. A cation antisite involves the substitution of an Am cation at the 16*d* Zr site and of a Zr cation at the 16*c* Am site. An oxygen Frenkel consists of a 48*f* vacancy and the occupation of an 8*a* site. The exact sequence of recombinations during the pyrochlore to fluorite order−disorder transition is still a matter of debate: anionic disorder followed by cationic recombination,[19] cationic disorder driving the transition,[20,21] or the concomitant occurrence of both cationic and anionic defects.[22] Although difficult to perform, studying partial disorder is therefore essential to understanding the underlying processes. To address this issue, we have characterized

(11) Rietveld, H. *J. Appl. Crystallogr.* **1969**, *2*, 65–71.
(12) Petricek, V.; Dusek, M.; Palatinus, L. *Jana 2000. The Crystallographic Computing System*; Institute of Physics: Praha, Czech Republic, 2000.
(13) Ravel, B.; Newville, M. *J. Synchrotron. Radiat.* **2005**, *12*, 537–541.
(14) Rehr, J.; Albers, R. C. *Rev. Mod. Phys.* **2000**, *72*, 621.
(15) Koningsberger, D.; Prins, R. *X-ray Absorption: Principles, Applications, Techniques of EXAFS, SEXAFS and XANES*; Wiley; New York, 1988.
(16) Chikalla, T.; Eyring, L. *J. Inorg. Nucl. Chem.* **1968**, *30*, 133–145.
(17) Sickafus, K.; Minervini, L.; Grimes, R.; Valdez, J.; Ishimaru, M.; Li, F.; McClellan, K.; Hartmann, T. *Science* **2000**, *289*, 748–751.
(18) Minervini, L.; Grimes, R.; Sickafus, K. E. *J. Am. Ceram. Soc.* **2000**, *83*, 1873–1878.
(19) Lian, J.; Weber, W.; Jiang, W.; Wang, L.; Boatner, L.; Ewing, R. *Nucl. Instrum. Methods Phys. Res., Sect. B* **2006**, *250*, 128–136.
(20) Hess, N.; Begg, B.; Conradson, S.; McCready, D.; Gassman, P.; Weber, W. *J. Phys. Chem. B* **2002**, *106*, 4663–4677.
(21) Chartier, A.; Meis, C.; Crocombette, J.; Weber, W.; Corrales, L. *Phys. Rev. Lett.* **2005**, 94.
(22) Sickafus, K.; Grimes, R.; Valdez, J.; Cleave, A.; Tang, M.; Ishimaru, M.; Corish, S.; Stanek, C.; Uberuaga, B. *Nat. Mater.* **2007**, *6*, 217–223.

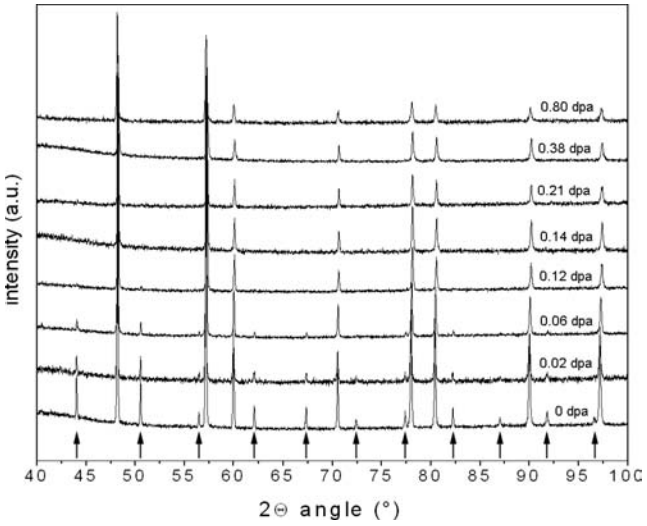

Figure 1. X-ray patterns for different dpa values showing the progressive loss of the pyrochlore superstructure starting at 0.02 dpa and completed after 0.21 dpa (arrows point to superstructure peaks).

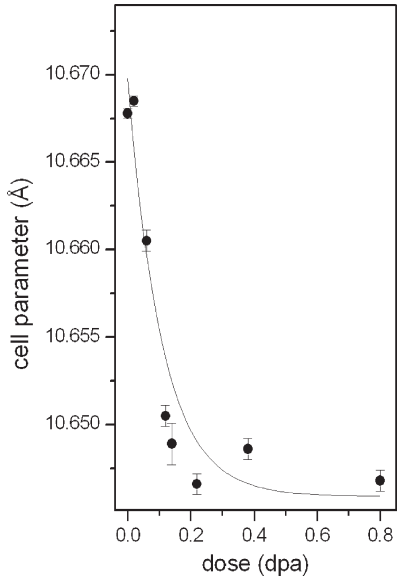

Figure 2. Decrease in the cell parameter as a function of displacements per atom (dpa).

short-lived intermediate states with XRD and XAS in addition to the initial and the defect-fluorite structure states.

X-ray profiles collected from the initial to the fluorite states were refined with the Rietveld method.[11] To obtain low isotropic displacement parameters for both Am and Zr, concomitant cation antisite and anion Frenkel pair defects had to be introduced to account for the progressive disorder occurring in both sublattices. A cation antisite is defined by $Am_{Am} + Zr_{Zr} \rightarrow Am_{Zr} + Zr_{Am}$, and an oxygen Frenkel is defined by $O_{O(48f)} \rightarrow V_{O(48f)} + O_{i(8a)}$. Accordingly, the 16*d* site was refined with Am_{Am}- and Zr_{Am}-type atoms and the 16*c* site with Am_{Zr}- and Zr_{Zr}-type atoms. In addition, oxygen originally at 48*f* was proportionally distributed to the 8*a* vacancy site ($O_{i(8a)}$). The O(8*b*) site was kept fully occupied (Table 1). Although oxygen is a much weaker scatterer of X-rays than either americium or zirconium, the displacement of oxygen atoms is quite reliable due to the particular characteristics of the pyrochlore structure. One of the two subsets constituting the diffraction pattern contains all of the information relative to the structural modifications creating the superstructure: O(48f) displacements and difference in scattering power between both cations sites.[23]

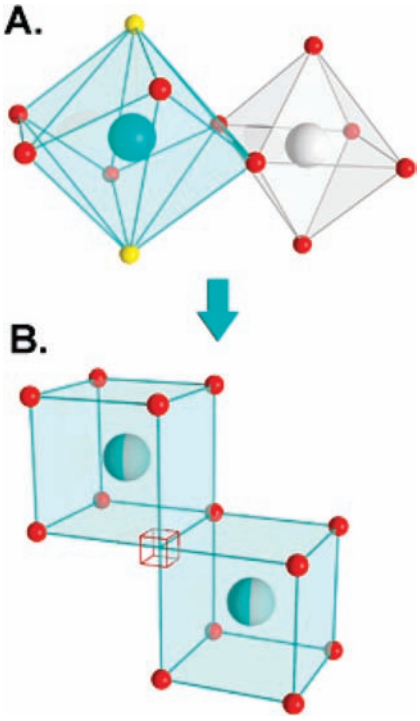

Figure 3. Coordination shells of Am and Zr cations in both structures. In the pyrochlore structure (A), Am (blue) is surrounded by two short-distance O(8*b*) atoms (yellow) and six longer-distance O(48*f*) atoms (red). Zr (gray) is surrounded by six equidistant O(48*f*)'s. In the defect-fluorite structure (B), both Am and Zr share the same crystallographic site, and O anions occupy 7/8 of a unique site.

While the initial state showed no cation exchange, the intermediate states revealed an increasing cationic disorder. Already after 0.02 dpa, 7% of the cations had swapped positions. This percentage increased to about 40% for 0.14 dpa and to 50% above 0.21 dpa, where the defect-fluorite state was reached. The increasing disorder during the transition is further revealed by the increase in the average O(48*f*) positional and displacement parameters. Once the defect-fluorite state was reached, disorder remained constant and the overall long-range order was maintained.

Cation disordering provides an opportunity to elucidate the cause of the volume contraction observed during the transition. We eliminated Am oxidation as a potential cause: the Am−L_{II} XANES (X-ray Absorption Near Edge Structure) spectrum showed no detectable amount of Am^{4+} up to 0.80 dpa (Figure 4). Instead, the progressive lattice contraction may be due to the smaller ionic radius of Am^{3+} at the 6-fold coordinated Zr site, occurring via Am−Zr antisite disorder, as compared to the larger radius in the initial 8-fold coordination. This result is in line with molecular dynamics simulations by Rushton et al.,[24] predicting negative volume changes for zirconate pyrochlores during the order−disorder transition, if r_A/r_B is between 1.48 and 1.57. Therefore, the cause for the volume contraction is most likely inherent to the ability of the structure to accommodate disorder and to form cation antisites.

(23) Wuensch, B.; Eberman, K. *JOM* **2000**, *52*, 19–21.
(24) Rushton, M.; Stanek, C.; Cleave, A.; Uberuaga, B.; Sickafus, K.; Grimes, R. *Nucl. Instrum. Methods Phys. Res., Sect. B* **2007**, *255*, 151–157.

Table 1. Details of the Rietveld Structure Refinements Including Site Occupation Fractions (SOF) and Isotropic Displacement Parameters $U_{iso}(Å^2)^a$

dpa	0	0.02	0.06	0.12	0.14	0.21	0.38	0.80
days after synthesis	0	40	100	200	250	370	650	1360
Space Group	$Fm\bar{3}m$	$Fm\bar{3}m$	$Fm\bar{3}m$	$Fm\bar{3}m$	$Fm\bar{3}m$	$Fm\bar{3}m$	$Fm\bar{3}m$	$Fm\bar{3}m$
a (Å)	10.6678(1)	10.6686(1)	10.6605(2)	10.6505(2)	10.6489(4)	5.3233(1)	5.3243(1)	5.3233(1)
R_p	3.38	5.83	3.53	3.12	4.03	5.11	4.60	4.74
R_{wp}	4.31	7.37	4.52	3.93	5.08	6.47	5.74	5.99
R_{Bragg}	3.18	2.34	2.42	2.22	3.27	1.94	2.05	3.24
GoF	1.28	1.11	1.30	1.17	1.12	1.17	1.38	1.08
SOF (Am_{Am}/Zr_{Zr})	0.986(1)	0.927(3)	0.804(3)	0.642(6)	0.62(1)			
SOF ($Zr_{Am}/Am_{Zr}/O_{i(8a)}$)	0.014(1)	0.073(3)	0.196(3)	0.357(6)	0.38(1)			
SOF ($O_{O(48f)}$)	0.9976(2)	0.9879(5)	0.9674(6)	0.941(1)	0.937(2)			
$x(O_{O(48f)})$	0.3372(7)	0.343(1)	0.367(1)	0.373(3)	0.368(5)			
$U_{iso}(Am_{Am}/Zr_{Am})$	0.0129(4)	0.016(1)	0.019(1)	0.021(1)	0.021(2)	0.026(1)	0.026(1)	0.018(2)
$U_{iso}(Zr_{Zr}/Am_{Zr})$	0.0121(6)	0.016(1)	0.021(1)	0.028(2)	0.026(3)	0.026(1)	0.026(1)	0.018(2)
$U_{iso}(O)$	0.044(2)	0.045(4)	0.057(2)	0.083(3)	0.088(5)	0.079(3)	0.074(3)	0.072(7)

[a] The following constraints were applied: identical SOF for Am_{Am} and Zr_{Zr}, as well as for Zr_{Am}, Am_{Zr}, and $O_{i(8a)}$, and all $U(O)$'s identical. The defect-fluorite patterns were refined in the $Fm\bar{3}m$ space group with only two sites. Thus, $Fm\bar{3}m$ SOF and $x(O_{O(48f)})$ values are meaningless in the corresponding columns.

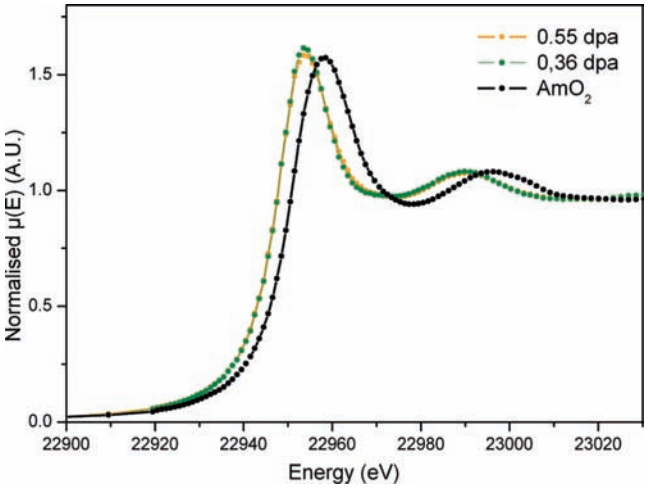

Figure 4. Am L_{II} normalized XANES spectra for the 0.36 and 0.55 dpa states and $Am^{4+}O_2$ reference sample.

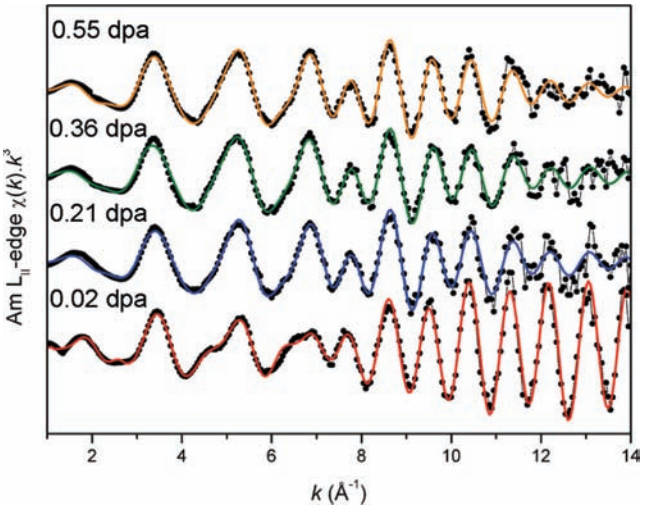

Figure 5. Am L_{II}-edge EXAFS spectra multiplied by k^3 for the 0.02, 0.21, 0.36, and 0.55 dpa states. Experimental data are displayed by symbols and fits by lines.

The local structure around both cations was then studied with Am L_{II} and Zr K-edges EXAFS (Extented X-ray Absorption Fine Structure) spectroscopy on four representative samples: one at 0.02 dpa, that is, still in an intermediate pyrochlore state, and three more at 0.21, 0.36, and 0.55 dpa in defect-fluorite states. EXAFS spectra are shown in Figures 5 and 6, Fourier transforms in Figures 7 and 8, and fit results in Table 2.

In line with the XRD results, we observe for the 0.02 dpa state identical Am−O(8*b*) and shorter Am−O(48*f*) distances in comparison to the initial structure, confirming the randomization of oxygen atoms through Frenkel pairs. This is further supported by the high Debye−Waller factors (σ^2), which reflect only static disorder since the samples were measured at 15 K. In contrast to americium, the local coordination around zirconium does not show any randomization of the oxygen sublattice (six equidistant O(48*f*) atoms at 2.13 Å and low σ^2). The ability of EXAFS to measure the expansion of selected bonds[25] offers complementary information on the disordering processes: while the Am−Am distance is in agreement with that of XRD, Am−Zr and Zr−Zr distances are shorter. However, Am−Zr

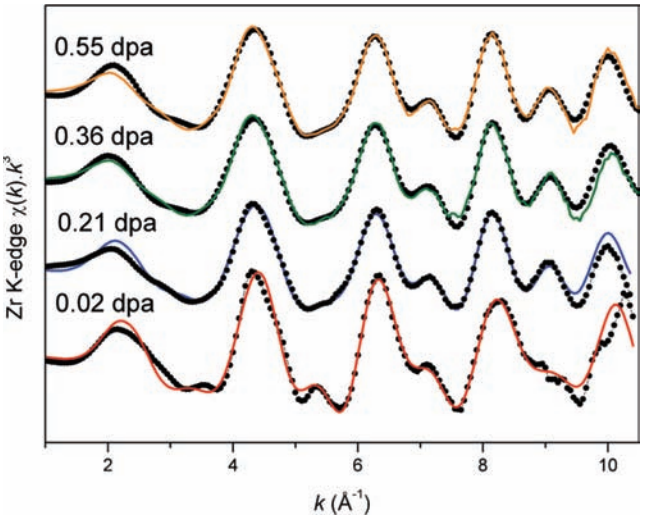

Figure 6. Zr K-edge EXAFS spectra multiplied by k^3 for the 0.02, 0.21, 0.36, and 0.55 dpa states. Experimental data are displayed by symbols and fits by lines.

(25) Howell, R.; Conradson, S.; Garcia-Adeva, A. *J. Phys. Chem. B* **2007**, *111*, 159–167.

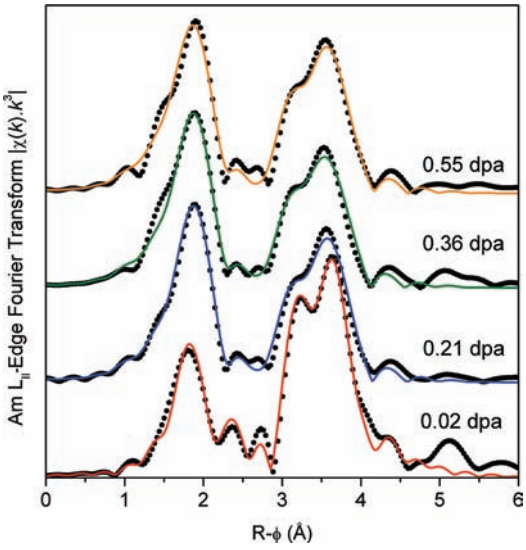

Figure 7. Am L_{II}-edge Fourier transform EXAFS spectra for the 0.02, 0.21, 0.36, and 0.55 dpa states. Experimental data are displayed by symbols and fits by lines. At 0.02 dpa, the two peaks at ~1.9 Å and ~2.2 Å correspond to the two Am−O distances (O(8*b*) and O(48*f*)) in the pyrochlore structure. A more intense peak at the shorter distance coupled with the fading peak at ~2.2 Å is indicative of the conversion to the fluorite structure (dpa ≥ 0.21), where Am is surrounded only by equidistant oxygen atoms.

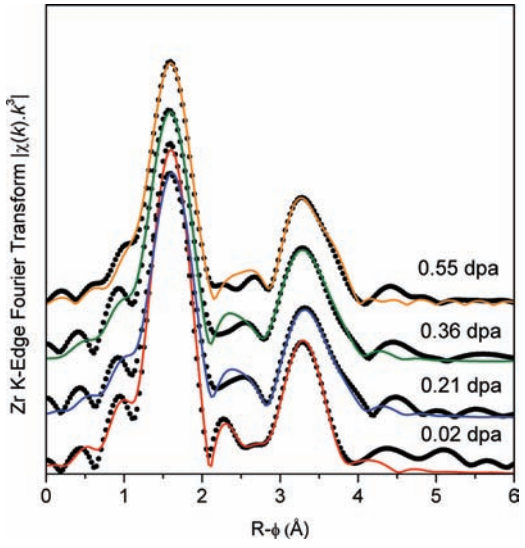

Figure 8. Zr K-edge Fourier transform EXAFS spectra for the 0.02, 0.21, 0.36, and 0.55 dpa states. Experimental data are displayed by symbols and fits by lines. The intense peak at ~1.6 Å corresponds to Zr−O distances and remains nearly identical for all of the spectra. The Zr−Am and Zr−Zr interactions give rise to the peak at ~3.3 Å, which broadens between 0.02 and 0.21 dpa because shells separate in distance.

(Am L_{II}-edge) and Zr−Am (Zr K-edge) distances are equal, providing evidence for the cation antisite formation in this intermediate structural state.

EXAFS spectra for the 0.21, 0.36, and 0.55 dpa fluorite states are nearly identical, demonstrating the stability of the defect-fluorite structure. Both Am and Zr cations are surrounded by only seven equidistant oxygen atoms, in comparison to the 8-fold coordination of the perfect fluorite structure. Along with the larger σ^2 in comparison to the 0.02 dpa pyrochlore, this gives ample evidence for the randomization of the oxygen sublattice and for a more disordered environment after the phase transition.

Table 2. Am L_{II} and Zr K-edges EXAFS Fit Results for 0.02, 0.21, 0.36, and 0.55 dpa States (R = Interatomic Distance in Å, CN = Coordination Number, σ^2 = Debye−Waller Factor in Å^2)[a]

		XRD	EXAFS		
		R (Å)	R (Å)	CN	σ^2 (Å^2)
Am−O(8*b*)	initial	2.3097(2)			
Fd$\bar{3}$*m*	0.02 dpa	2.3098(2)	2.31(2)	2.8(5)	0.006(1)
Am−O(48*f*)	initial	2.563(5)			
Fd$\bar{3}$*m*	0.02 dpa	2.52(1)	2.53(2)	4.8(5)	0.015(1)
Am−O(8*c*)	0.21 dpa	2.3050(4)	2.35(2)	6.6(5)	0.009(1)
Fm$\bar{3}$*m*	0.36 dpa		2.36(1)	7.0(5)	0.011(1)
	0.55 dpa		2.36(1)	7.0(5)	0.011(1)
Am−Am	initial	3.7716(4)			
	0.02 dpa	3.7719(4)	3.76(1)	6.0(5)	0.004(1)
	0.21 dpa	3.7641(7)	3.75(1)	5.2(5)	0.007(1)
	0.36 dpa		3.75(1)	6.0(5)	0.009(1)
	0.55 dpa		3.75(1)	6.0(5)	0.010(1)
Am−Zr	initial	3.7716(4)			
	0.02 dpa	3.7719(4)	3.74(1)	6.0(5)	0.008(1)
	0.21 dpa	3.7641(7)	3.65(1)	6.3(5)	0.012(1)
	0.36 dpa		3.64(1)	6.0(5)	0.011(1)
	0.55 dpa		3.65(1)	6.0(5)	0.011(1)
Am−O(48*f*)	initial	4.318(2)			
	0.02 dpa	4.332(4)	4.26(4)	17(2)	0.01(1)
Zr−O(48*f*)	initial	2.103(3)			
Fd$\bar{3}$*m*	0.02 dpa	2.131(7)	2.13(1)	6.3(5)	0.005(1)
Zr−O(8*c*)	0.21 dpa	2.3050(4)	2.15(1)	6.6(5)	0.008(1)
Fm$\bar{3}$*m*	0.36 dpa		2.14(1)	6.7(5)	0.008(1)
	0.55 dpa		2.15(1)	7.5(5)	0.008(1)
Zr−Am	initial	3.7716(4)			
	0.02 dpa	3.7719(4)	3.75(2)	6(1)	0.004(1)
	0.21 dpa	3.7641(7)	3.64(2)	6(1)	0.010(1)
	0.36 dpa		3.64(2)	6(1)	0.011(1)
	0.55 dpa		3.64(2)	6(1)	0.010(1)
Zr−Zr	initial	3.7716(4)			
	0.02 dpa	3.7719(4)	3.75(2)	6(1)	0.008(1)
	0.21 dpa	3.7641(7)	3.51(2)	6(1)	0.017(1)
	0.36 dpa		3.51(2)	6(1)	0.015(1)
	0.55 dpa		3.52(2)	6(1)	0.015(1)

[a] For comparison, interatomic distances obtained from the XRD Rietveld refinement are reported at initial, 0.02 and 0.21 dpa states.

The Am−O distance of 2.36 Å is higher than that derived from the defect-fluorite XRD structural model; however, it is in agreement with the distance observed in 30 wt % Am-doped, yttria-stabilized zirconia.[26] Since both Am and Zr cations occupy the same crystallographic position in the fluorite structure lattice (see Figure 3), the same oxygen distance for both the Am and Zr coordination spheres was expected. Surprisingly, the Zr−O distance of 2.15 Å is much shorter than the Am−O distance. Li et al. observed a similar Zr−O distance for 7-fold-coordinated polyhedra in cubic stabilized zirconia.[27] The Zr−O distance remains always close to the distances of the initial states, that is, is almost unaffected by irradiation. Another evolution in the defect-fluorite structure is the disorder observed for the cation−cation coordination shells reflected by the very high σ^2 values, in particular for zirconium. From the detailed analysis of distances, important conclusions become apparent. While the Am−Am distances are in agreement with XRD, the Am−Zr and Zr−Zr distances are shorter, implying that the Am and Zr local environments are nonequivalent. For all

(26) Walter, M.; Nastren, C.; Somers, J.; Jardin, R.; Denecke, M. A.; Brendebach, B. *J. Solid State Chem.* **2007**, *180*, 3130–3135.
(27) Li, P.; Chen, I.; Penner-Hahn, J. *J. Am. Ceram. Soc.* **1994**, *77*, 118–128.

irradiation levels, Am−Zr and Zr−Am distances are identical, in line with the cation antisite formation. As proposed by earlier studies,[20,28] such a disorder in the Zr cation shell reveals a loss of second-neighbor periodicity due to rotations of the Zr polyhedra along shared edges and corners. This polyhedral flexibility thereby contributes to accommodating the increasing disorder within the structure.

Conclusion

Our work provides experimental insight into the disordering processes occurring in $Am_2Zr_2O_7$ when subjected to α self-irradiation. The compound is extremely radiation-tolerant and free from swelling due to the simultaneous formation of cation antisites and oxygen Frenkel pairs. While XRD results established that the overall long-range order is maintained, EXAFS provided complementary information on the disordering processes. The stability of the Zr−O bond and rotations of Zr polyhedra may be the key to the unusual properties of this phase.

Acknowledgment. We thank E. Gavilan and A. Pieragnoli for their support at the European Synchrotron Radiation Facility (ESRF) during EXAFS and C. Belin for assistance in X-ray data analysis. The authors are grateful to the MATAV ceramics basic research programme of the CEA for supporting this work and to the European Synchrotron Radiation Facility for provision of synchrotron radiation facilities.

(28) Ewing, R.; Chakoumakos, B.; Lumpkin, G.; Murakami, T.; Greegor, R.; Lytle, F. *Nucl. Instrum. Methods Phys. Res., Sect. B* **1988**, *32*, 487–497.